Supplementary Information (SI) for Chemical Science.
This journal is © The Royal Society of Chemistry 2026

Supporting Information

Non-Ideal Stoichiometry and Thermochemistry of Aqueous Iridium Oxide Nanoparticles in Proton-Coupled Electron Transfer and Oxygen-Atom Transfer

Justin L. Lee, Saeed Saeed, James M. Mayer*

james.mayer@yale.edu
Department of Chemistry, Yale University, New Haven, Connecticut 06520-8107, United States

Table of Contents

Section S1: General considerations

S1.1 Reagents

18 MΩ cm water (H_2O) from a Synergy® Milli-Q system was used in all studies. H_2O and D_2O (Sigma-Aldrich, 99.9% enrichment) were sparged with nitrogen gas for > 1 min/mL to remove ambient air and transported into a nitrogen-filled glovebox prior to use. All reagents were used as received unless otherwise stated. K_2IrCl_6 (99.99% trace metals) was purchased from Sigma-Aldrich. Proton-coupled electron transfer (PCET) reagents 1,4-hydroquinone (H_2Q, ReagentPlus, >99.5%), *p*-benzoquinone (Q, reagent grade, >98%), and (+)-sodium L-ascorbate (NaAscH, 99%+) were purchased from Sigma-Aldrich. Potassium hydrogen monopersulfate (oxone) was purchased from EMD Millipore Corporation. Oxygen atom transfer reagents $NaNO_2$ (ACS reagent), bis(p-sulfonatophenyl)phenylphosphine dihydrate dipotassium salt (PAr_3, 97%), and pyridine (Py, 99.8%) were purchased from Sigma-Aldrich. Isotope experiments used D_2O (Sigma-Aldrich, 99.9% enrichment), $Na^{15}NO_2$ (ICON Isotopes, 99% enrichment) and $Na^{15}NO_3$ (Sigma-Aldrich, >98% enrichment).

S1.2 Instrumentation

Transmission electron microscopy images of the nanoparticles (NPs) were measured with a FEI Tecnai Osiris 200 kV TEM. As-prepared IrO_x NPs (~1.7 mM [Ir]) was deposited onto the same type of grid. All UV-vis spectra were collected using a Cary 5000 spectrophotometer with a scanning monochromator inside a nitrogen-filled glovebox (equipped with Ocean Optics fiber optics cables). pH measurements were collected using a Thermo Scientific™ Orion™ PerpHecT™ ROSS™ Combination pH Micro Electrode inside the glove box (other than during NP syntheses), calibrated using five NIST pH standard solutions in H_2O from BrandNu: 1.68, 4.01, 7.00, 10.01, 12.46. Inductively coupled plasma mass spectrometry was performed on a Perkin-Elmer ICP-MS Elan DRC-e. ^{1}H, ^{15}N, and ^{31}P NMR spectra were collected on an Agilent DD2 400 MHz and 500 MHz NMR spectrometers at room temperature. $(CH_3)_2SO_2$ (δ 3.14 ppm) or *tert*-butyl alcohol (δ 1.24) was used as the internal ^{1}H standard. Cyclic voltammetry was performed on a CH Instruments model 650D Potentiostat in a nitrogen-filled glovebox, using a standard 3-electrode setup. A 3 mm-diameter boron-doped diamond (BDD) working electrode, a platinum wire counter electrode, and an Ag/AgCl reference electrode (BASi Research Products) were used. The UV-vis spectroelectrochemistry setup is detailed in Section S5. All voltammograms were converted from the Ag/AgCl reference to NHE (+0.21 V) as an internal standard. All measurements are at room temperature. pH adjustments were done *via* simple dilution with 18 MΩ H_2O, or with diluted (~100 mM) HNO_3 or NaOH.

Section S2: IrO_x synthesis & characterization

IrO_x NPs were prepared following a previously reported procedure.[1] 0.0971 g K_2IrCl_6 was dissolved in 100 mL 18 MΩ cm H_2O to give an orange-brown solution, and 8.000 mL 10% w/w NaOH (aq, 0.0200 mol NaOH) was added to increase the pH to 13.0. The reaction mixture was heated at 90 °C for 20 minutes to produce a pale blue color, and then cooled in an ice bath. 8.500 mL 3 M HNO_3 (aq, 0.0255 mol HNO_3) was added to the mixture to produce a dark purple color (Figure S1) and decrease the pH to 1.45, and the reaction mixture was allowed to stir at 0 °C for 80 minutes. The colloidal solution was degassed for ~2.5 hours under a stream of nitrogen gas then transported into the glovebox for storage and all measurements. The solution pH of the as-prepared IrO_x NPs was ~1.65.

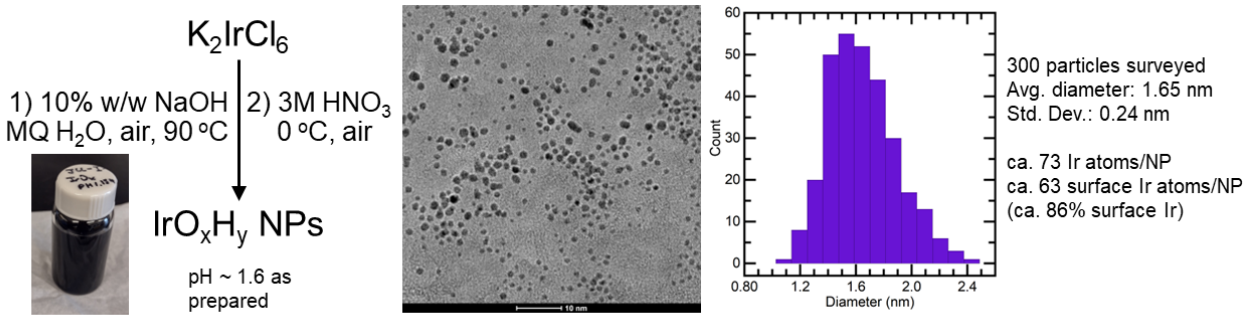

Figure S1. Basifying then acid hydrolysis of K_2IrCl_6 produced a dark purple colloidal suspension of IrO_x NPs. TEM images of the IrO_x NPs illustrated the spherical shape of the NPs, with an average diameter of 1.7±0.2 nm. The scale bar is 10 nm. Reproduced from Lee, J. L.; Gentry, N. E.; Peper, J. L.; Hetzel, S.; Quist, C.; Menges, F. S.; Mayer, J. M. *ACS Nano* **2025**, *19*, 10289–10300. Copyright 2025 American Chemical Society.[2]

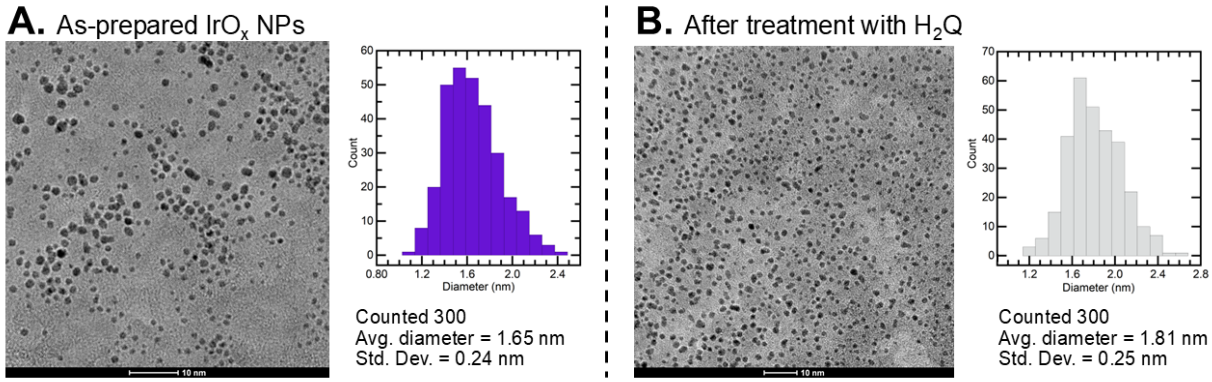

Figure S2. TEM images of the IrO_x NPs before (**A**) [same as in Figure S1] and after (**B**) treatment with H_2Q (1 mL of the as-prepared IrO_x + 0.8 μmol H_2Q, 1.2 equiv. H_2Q using the 2 oxidizing equivalents : 1 H_2Q ratio) after 5 hours. A small increase in NP diameter was observed. The scale bars are 10 nm.

ICP-MS was performed to determine the [Ir] concentration of the colloidal solution. 1.000 mL of the as-prepared IrO_x NPs were digested with 4.000 mL aqua regia (4:1 HCl:HNO_3 [concentrated acids]) for 3 days, then further diluted 2000-fold *via* serial dilutions using 1% HNO_3 (aq); the total dilution was 10,000-fold. An Ir ICP-MS calibration curve was prepared using known diluted samples of an Ir standard, and the [Ir] of the colloidal solution was found to be 1.682±0.007 mM in 3 samples (Figure S3), which is in good agreement with the expected [Ir] of 1.743 mM (96.5 %) from the amount of initial material used.

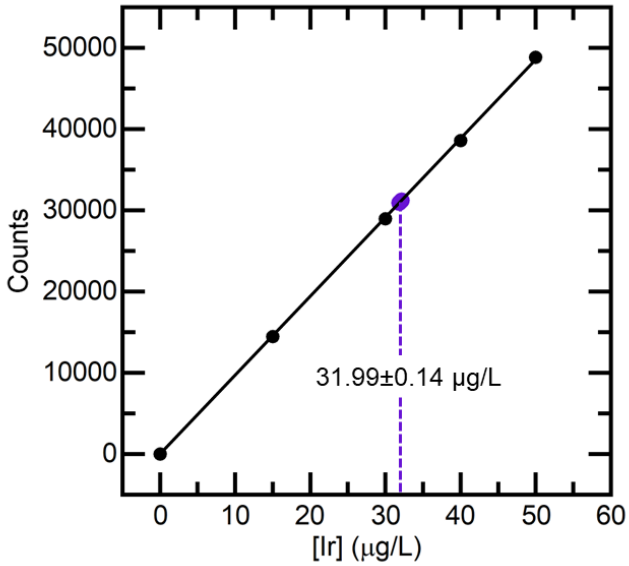

Figure S3. ICP-MS quantification of [Ir] content in IrO_x NP samples. The IrO_x solution was digested by aqua regia then diluted in 1% HNO_3 (aq) (total 10,000-fold dilution). 31.99±0.14 μg/L [Ir] was measured by ICP-MS. The undiluted NP sample is calculated to contain 319900±1400 μg/L [Ir], or 1.682 mM [Ir]. This is in good agreement with the expected [Ir], 1.743 mM. Reproduced from Lee, J. L.; Gentry, N. E.; Peper, J. L.; Hetzel, S.; Quist, C.; Menges, F. S.; Mayer, J. M. *ACS Nano* **2025**, *19*, 10289–10300. Copyright 2025 American Chemical Society.[2]

TEM imaging determined the diameter of the NPs to be 1.65±0.24 nm (Figure S1). Based on the measured NP average radius (r_{NP} = diameter/2 = 1.65 nm/2 = 0.825 nm) and the density of rutile IrO_2 (11.66 g cm^{-3}) as an approximation, each IrO_x NP is calculated to contain ~73 Ir atoms (eqs. S1, S2, S3).

$$(4/3)\pi r_{NP}^3 \times \text{density} = (4/3)\pi(8.25 \times 10^{-8}\ \text{cm})^3 \times (11.66\ \text{g cm}^{-3}) = 2.74 \times 10^{-20}\ \text{g per NP} \quad \text{eq. S1}$$

$$(2.74 \times 10^{-20}\ \text{g per NP}) / (224.22\ \text{g } IrO_2\ \text{mol}^{-1}) = 1.22 \times 10^{-22}\ \text{mol } IrO_2\ \text{per NP} \quad \text{eq. S2}$$

$$(1.22 \times 10^{-22}\ \text{mol } IrO_2\ \text{per NP}) * (1\ \text{mol Ir})/(1\ \text{mol } IrO_2) * (6.022 \times 10^{23}\ \text{atoms Ir/mol Ir})$$

$$= 73\ \text{atoms Ir per NP} \quad \text{eq. S3}$$

The number of surface Ir atoms is estimated by assuming the thickness of the surface layer is the length of a typical Ir–O which is estimated as 0.20 nm.[3] The volume of the surface ($V_{surface}$) was calculated (eq. S4) by subtracting the volume of the spherical NP (V_{NP}) by the volume of the bulk (V_{bulk}).

$$V_{surface} = V_{NP} - V_{bulk} \quad \text{eq. S4}$$

The surface layer thickness is defined as within one Ir–O bond. Therefore, the radius of the spherical bulk (r_{bulk}) is 2 Ir–O bonds shorter than r_{NP} (eq. S5).

$$r_{bulk} = r_{NP} - [2 \times d(\text{Ir–O})] = r_{NP} - (2 \times 0.199\ \text{nm}) \quad \text{eq. S5}$$

The volume of the surface ($V_{surface}$) can therefore be calculated to be 2.03 nm^3 (eq. S6).

$$V_{surface} = V_{NP} - V_{bulk}$$

$$V_{surface} = (4/3)\pi r_{NP}^3 - (4/3)\pi r_{bulk}^3 = (4/3)\pi(0.825\ \text{nm})^3 - (4/3)\pi(0.825\ \text{nm} - 2 \times 0.199\ \text{nm})^3$$

$$= (4/3)\pi(0.825\ \text{nm})^3 - (4/3)\pi(0.825\ \text{nm} - 2 \times 0.199\ \text{nm})^3$$

$$= 2.03\ \text{nm}^3 \quad \text{eq. S6}$$

$V_{surface}$ is 86% of V_{NP} (eq. S7), so the surface should contain 63 Ir atoms (eq. S8). Alternatively, the unit cell volume of IrO_2 (V_{uc} = 0.0645 nm^3) and the number of Ir atoms per IrO_2 unit cell (2) can be used to calculate 63 Ir atoms on the surface (eqs. S9, S10).

$$V_{surface} / V_{NP} = 0.86 \quad \text{eq. S7}$$

$$73\ \text{Ir atoms per NP} * 0.86 = 63\ \text{Ir atoms per NP surface} \quad \text{eq. S8}$$

$$V_{surface} / V_{uc} = (2.03\ \text{nm}^3) / (0.0645\ \text{nm}^3\ \text{per unit cell}) = 31.5\ \text{unit cells on the surface} \quad \text{eq. S9}$$

$$(31.5\ \text{unit cells on the surface}) * (2\ \text{Ir atoms per unit cell}) = 63.0\ \text{Ir atoms per NP surface} \quad \text{eq. S10}$$

Section S3: Electrochemical measurements of the IrO_x NPs

The full electrochemical window of the cyclic voltammetry measurement of the IrO_x NPs is shown in Figure S4. A Pt electrode was used as the working electrode; Pt wire as the counter electrode; and Ag/AgCl electrode as the reference electrode. The pH was adjusted to pH 1.89 using a ~120 mM $NaOH_{(aq)}$ solution. Two PCET processes – $Ir^{5+/4+}$ and $Ir^{4+/3+}$ – were observed, but only the latter process is examined in this study.

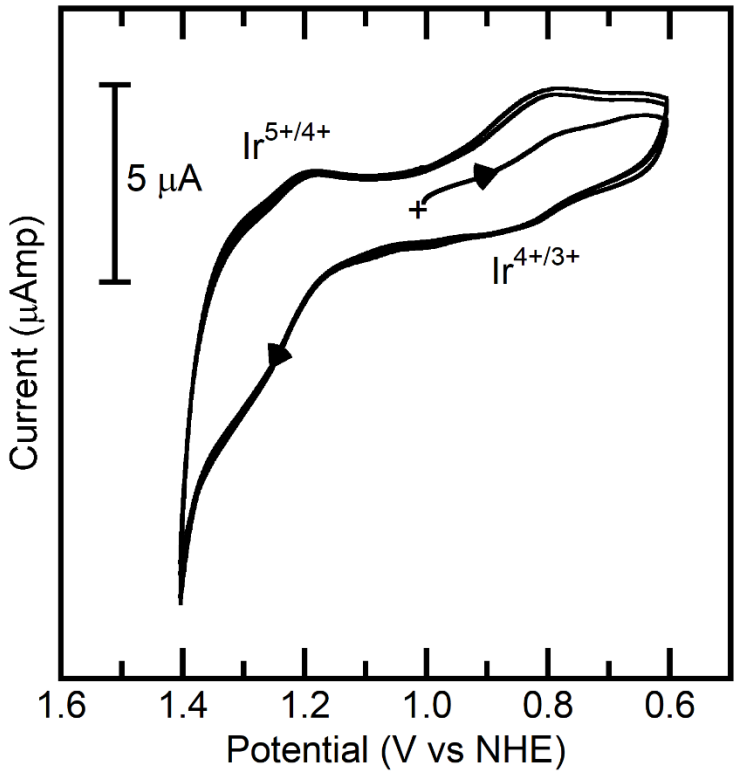

Figure S4. Full electrochemical window of the cyclic voltammogram of IrO_x NPs. The as-prepared colloids were basified to pH 1.89 using $NaOH_{(aq)}$, and the cyclic voltammogram was collected at a scan rate of 20 mV s^{-1} at room temperature. A Pt electrode was used as the working electrode; Pt wire as the counter electrode; and Ag/AgCl electrode as the reference electrode. + indicates the open circuit potential.

pH-dependent cyclic voltammetry measurements were performed on the as-prepared IrO_x NPs ([Ir] = 1.7 mM before dilution from basification). A boron-doped diamond electrode was used as the working electrode; Pt wire as the counter electrode; and Ag/AgCl electrode as the reference electrode. pH adjustment (pH 1.56 to 3.95) was achieved using a ~100 mM $NaOH_{(aq)}$ solution. Above pH > 4, the colloids aggregated over time, presumably due to decreasing electrostatic interactions to stabilize the nanoparticles. A selected number of voltammograms is illustrated in Figure 4A of the main text, which shows the $E_{1/2}$ of the $Ir^{4+/3+}$ redox process shifts cathodically as the pH increases. The $E_{1/2}$ values from 32 data points are tabulated and used to construct a Pourbaix diagram in Figure 4B of the main text.

Section S4: UV-vis and ^1H NMR titrations

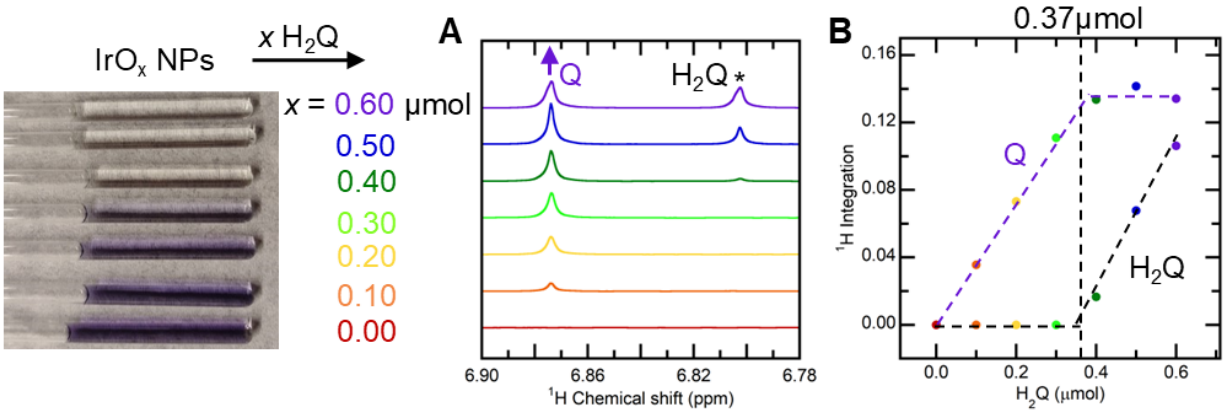

Figure S5. NMR titrations of IrO_x NPs with aliquots (0.10 µmol) of hydroquinone (H_2Q); the solvent was 83:17 H_2O:D_2O; $(CH_3)_2SO_2$ was used as an internal chemical shift (δ 3.14 ppm) and quantification reference. Addition of H_2Q results in the growth of the benzoquinone (Q) features (indicated by the purple arrows) in the ^1H NMR spectra (**A**). The asterisks (*) indicate excess Q. The integrations of the δ 6.87 ppm feature for Q and δ 6.80 ppm feature for H_2Q are plotted in a Beer's law plot to quantify the oxidizing equivalents of IrO_x (**B**).

Data from UV-vis titrations of as-prepared IrO_x NPs with H_2Q, $[Co^{II}(bpy)_3]^{2+}$, ascorbic acid ($AscH_2$), and sodium ascorbate (Na^+AscH^-) are shown in Figures S6-S9.

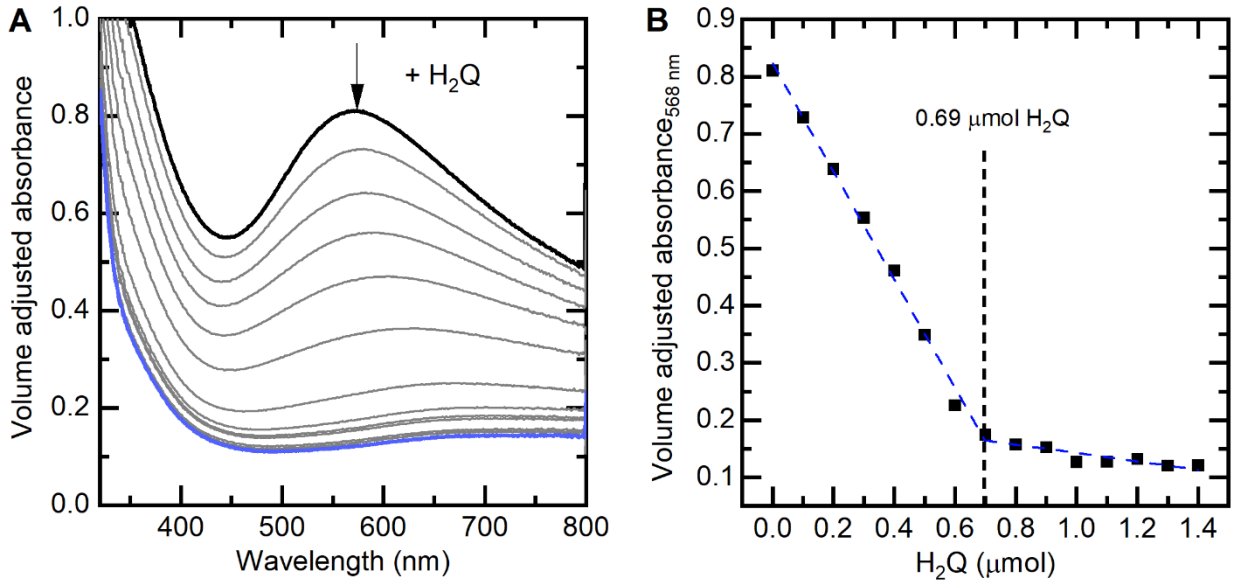

Figure S6. (**A**) Spectra from a UV-vis titration of IrO_x+H_2Q obtained from concurrent pH measurements discussed in Section II.B.3 of the main text. (**B**) Beer's Law plot of volume-corrected A_{568} *vs.* µmol of H_2Q added.

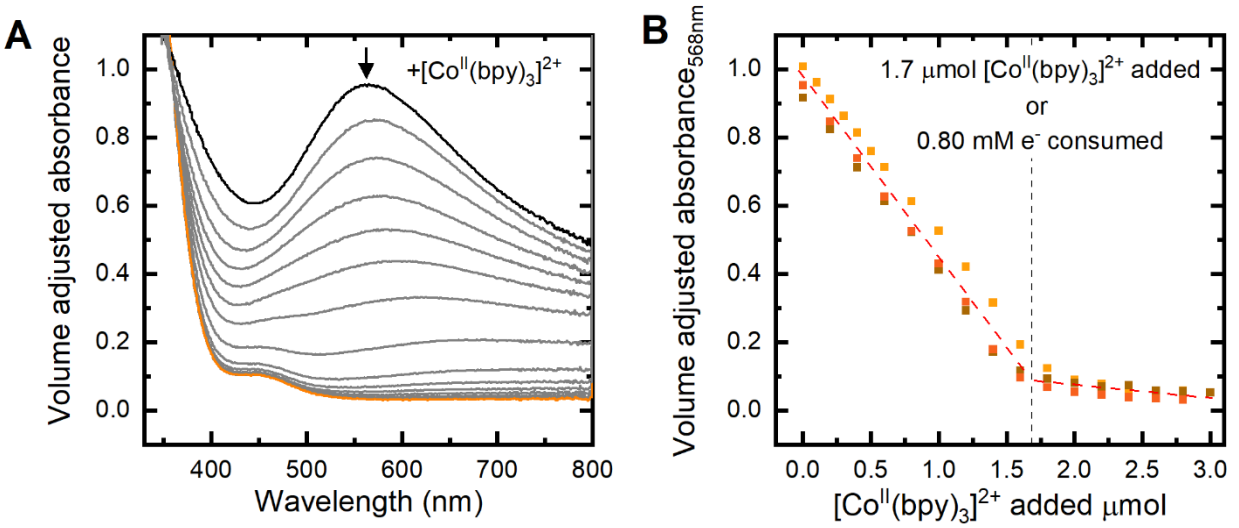

Figure S7. (**A**) UV-vis titration of IrO_x NPs in H_2O (2-fold diluted from the as-prepared NP batch) with $[Co^{II}(bpy)_3]^{2+}$. Aliquots of $[Co^{II}(bpy)_3]^{2+}$(0.2 µmol) result in incremental decrease of the IrO_x optical absorbance. (**B**) Beer's law plot is used to quantify the oxidizing equivalents of IrO_x NPs. The three different shades of orange represent three separate titrations of IrO_x NPs with $[Co^{II}(bpy)_3]^{2+}$.

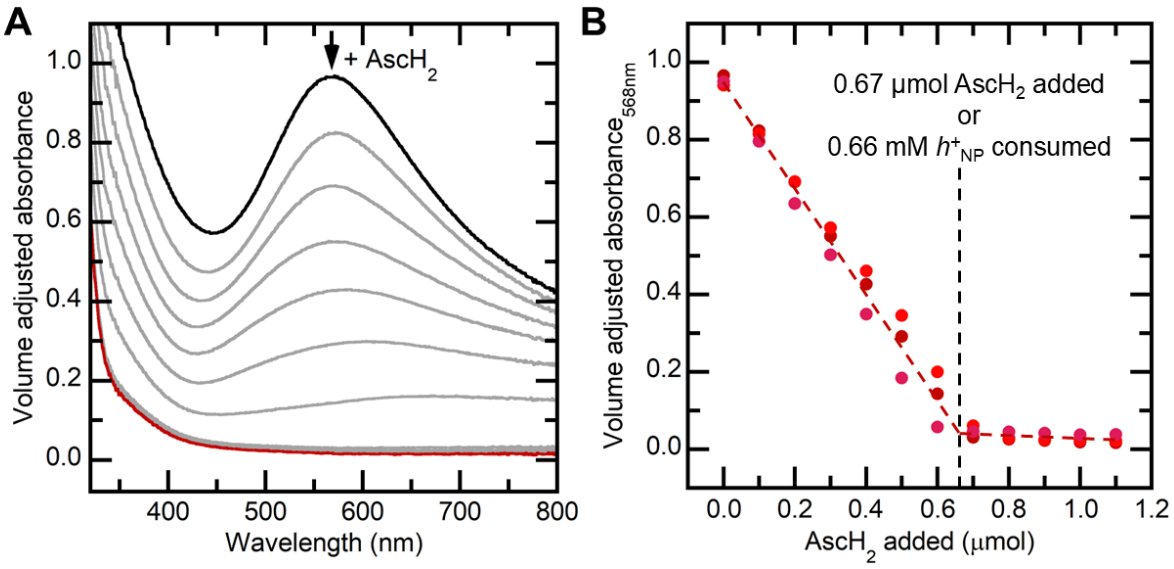

Figure S8. (**A**) UV-vis titration of IrO_x NPs in H_2O (2-fold diluted from the as-prepared NP batch) with a solution of ascorbic acid ($AscH_2$). Aliquots of $AscH_2$ (0.1 µmol) result in incremental decrease of the IrO_x optical absorbance. (**B**) Beer's law plot is used to quantify the oxidizing equivalents of IrO_x NPs. The three different shades of red represent three separate titrations of IrO_x NPs with $AscH_2$.

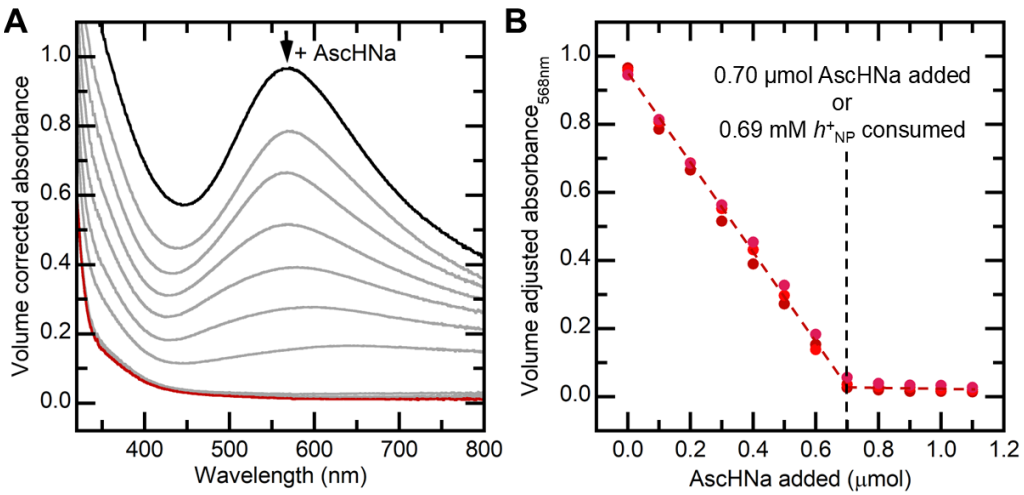

Figure S9. (**A**) UV-vis titration of IrO_x NPs in H_2O (2-fold diluted from the as-prepared NP batch) with a solution of sodium ascorbate (NaAscH). Aliquots of NaAscH (0.1 µmol) result in incremental decrease of the IrO_x optical absorbance. (**B**) Beer's law plot is used to quantify the oxidizing equivalents of IrO_x NPs. The three different shades of red represent three separate titrations of IrO_x NPs with NaAscH.

The main text shows a titration of IrO_x + H_2Q monitored by pH. Similar experiments were attempted with $AscH_2$, $AscH^-$ (Figure S10), and $[Co^{II}(bpy)_3]^{2+}$. The $AscH^-$ was immediately protonated to $AscH_2$ under the titration conditions of pH 1.86. The results were roughly consistent with the H_2Q titration. However, other observations of $[Co^{II}(bpy)_3]^{2+}$ in acid solutions suggested the possibility of loss of bpy on the timescale of the titration, which would prevent simple interpretation of the pH data in terms of IrO_x proton stoichiometry. In the same vein, ascorbic acid is a more complicated reductant than the obligate $2e^-$,$2H^+$ H_2Q, as it can undergo self-condensation and other reactions.[4–6] Therefore, while two initial experiments are shown below, these titrations were not pursued.

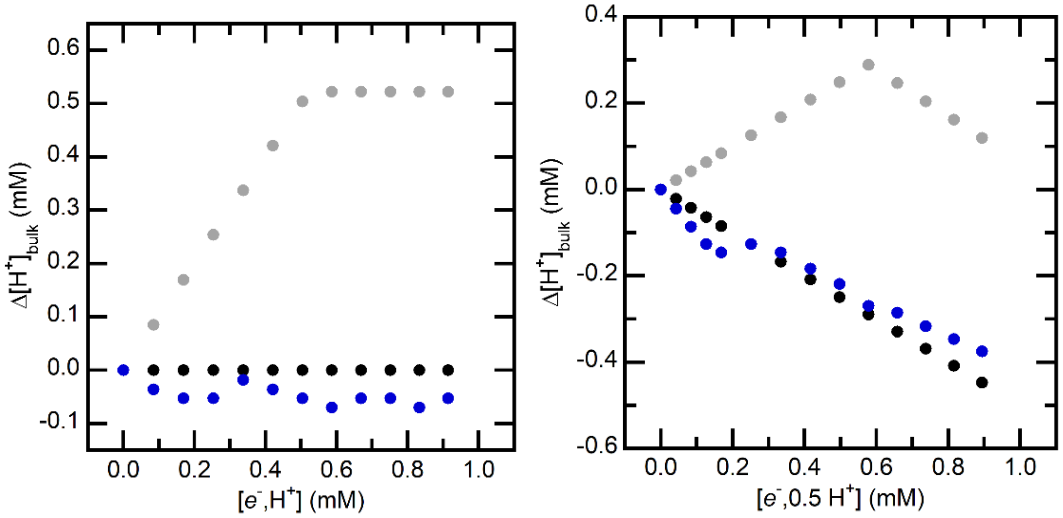

Figure S10. Preliminary pH titrations of as-prepared IrO_x NPs with $AscH_2$ (left) and $AscH^-$ (right). The blue points are the experimental results; gray and black points are the $\Delta[H^+]$ values predicted if the reagents only added e^- or $1e^-$+$1H^+$, respectively.

UV-Vis titrations of as-prepared IrO_x NPs with Na_2SO_4, oxone, and KI.

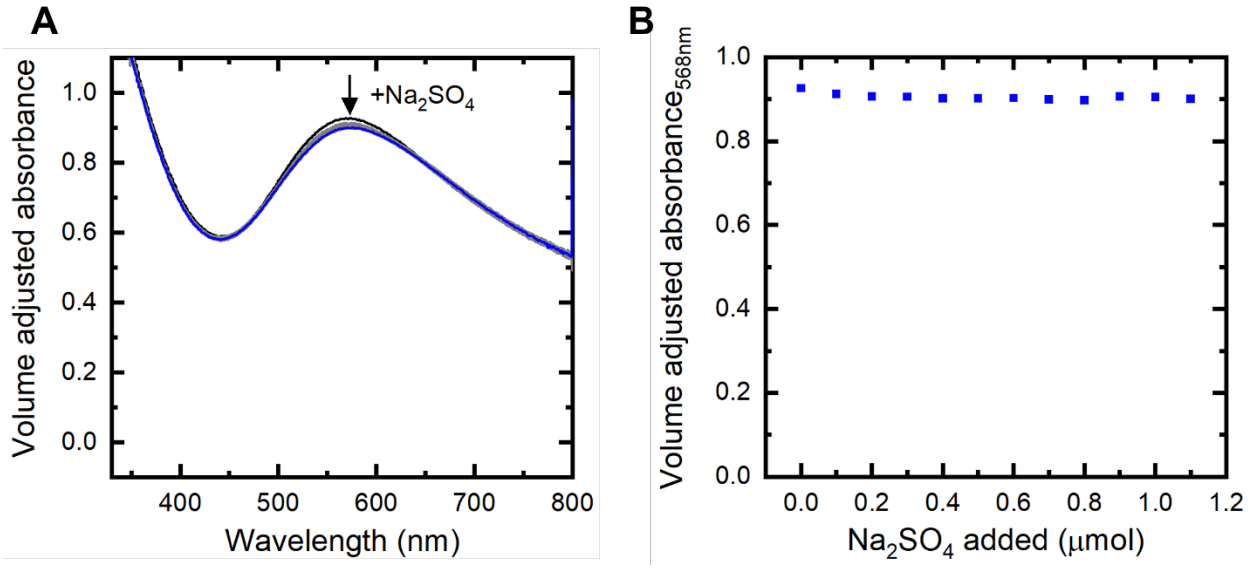

Figure S11. (**A**) UV-vis titration of IrO_x NPs in H_2O (2-fold diluted from the as-prepared NP batch) with Na_2SO_4. (**B**) 568 nm absorbance changes during the incremental addition of Na_2SO_4 aliquots, showing little change.

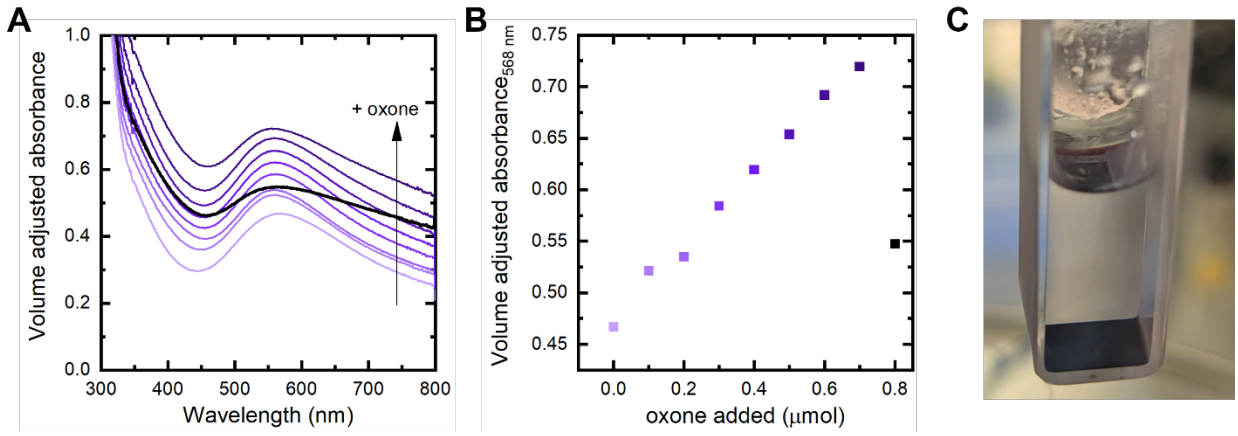

Figure S12. (**A**) UV-Vis titration of as-prepared IrO_x NPs in H_2O (4-fold diluted from the as-prepared NP batch) with oxone. Black spectrum indication final aliquot added, showing a decrease in the absorbance. (**B**) Beer's law plot showing the drop in absorbance at 568 nm once 0.8 μmol of oxone is added. (**C**) Optical image of IrO_x NPs after 0.8 μmol of oxone is added, with particles no longer in a colloidal suspension. The dark region at the bottom of the cuvette is the precipitated, oxidized NPs.

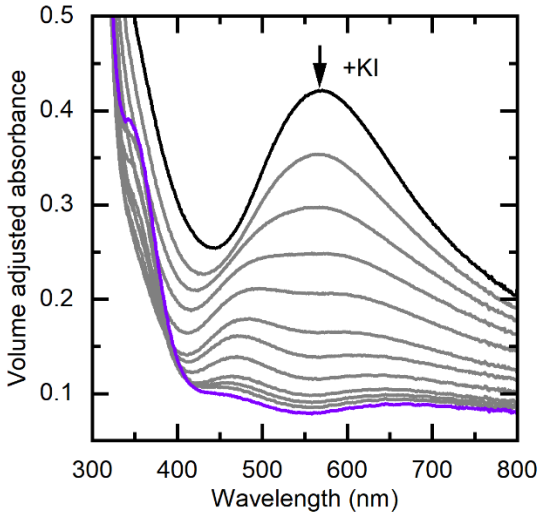

Figure S13. UV-vis titration of IrO_x NPs in H_2O (2-fold diluted from the as-prepared NP batch) with KI. Aliquots of KI (0.1 µmol) result in incremental decrease of the IrO_x optical absorbance.

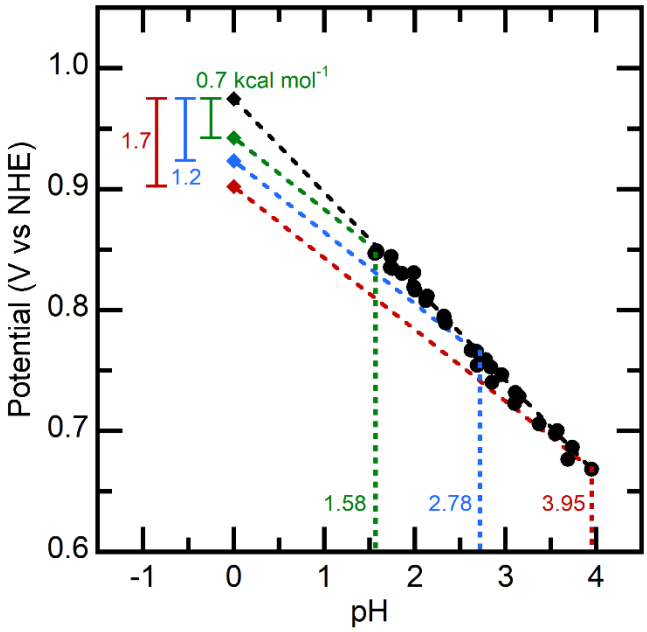

Figure S14. Extrapolating the E° using the -79 mV/pH slope (black), using the -59 slope from pH 1.58 (green), from pH 2.78 (blue), from pH 3.95 (red).

Section S5: Experimental details for UV-vis spectroelectrochemistry

UV-vis spectroelectrochemistry was performed using the Cary5000 spectrophotometer in conjunction with a Pine Research Honeycomb Spectroelectrochemistry setup, which consisted of a patterned "honeycomb" electrode mounted inside a thin-layer quartz cuvette (1.7 mm pathlength, Figure S15). The "honeycomb" electrode was Pt-based, and an Ag/AgCl reference electrode was also used. All voltammograms were converted from the Ag/AgCl reference to NHE (+0.21 V) as an internal standard. All measurements are at room temperature. pH adjustments were done with diluted (~100 mM) NaOH.

Figure S15. The Pine Research Honeycomb spectroelectrochemistry cell used in this study. The quartz cuvette has a 1.7 mm pathlength. The patterned "honeycomb" electrode is Pt-based, and an external Ag/AgCl reference electrode was also used.

1.5 mL IrO_x NP solution was added to the cuvette, and the "honeycomb" and Ag/AgCl reference electrodes were assembled inside the cell. Controlled potential electrolysis was performed at applied potentials ($E_{applied}$) ranging from 0.53 to 1.13 V vs NHE at 0.025 V intervals (Figure 5A of the main text). Under a potential bias, the charge passed was monitored until it reached plateau. Simultaneously, the UV-vis spectra of the electrolyzed colloids were recorded at 2-minute intervals, until the spectra stopped changing. The optical spectra at different applied potentials are compared in Figure 5B. The colloids' absorbance at 568 nm was converted to a H-atom surface coverage ($\theta_{\mathbf{H}}$) using the chemical titration values that previously determined the oxidizing equivalents in the IrO_x NPs (e.g., Figure 1). θ_H was then plotted against $E_{applied}$ in Figure 5C to produce the H-atom binding isotherm. The experimental data (colored circles) was fitted with the Frumkin isotherm (eq. 15) using Igor Pro 9. $E°_{isotherm}$ and C were set as the variables, yielding $E°_{isotherm}$ = 1.01 V vs NHE (BDFE([IrO_x]–H) = 76 kcal mol^{-1}) and C = 0.28 V (6.5 kcal mol^{-1}).

The redox reversibility of the colloids was tested under the spectroelectrochemistry experimental conditions (Figure S16). The NPs were cycled between applied potentials of 0.56 and

1.07 V vs NHE, and their optical spectra were recorded (Figure S16A). The absorbance at 568 nm showed only a small deviation after 4 cycles (Figure S16B), demonstrating the redox reversibility of the NPs similar to the chemical treatment with H_2Q / $NaIO_3$ (Figure 2).

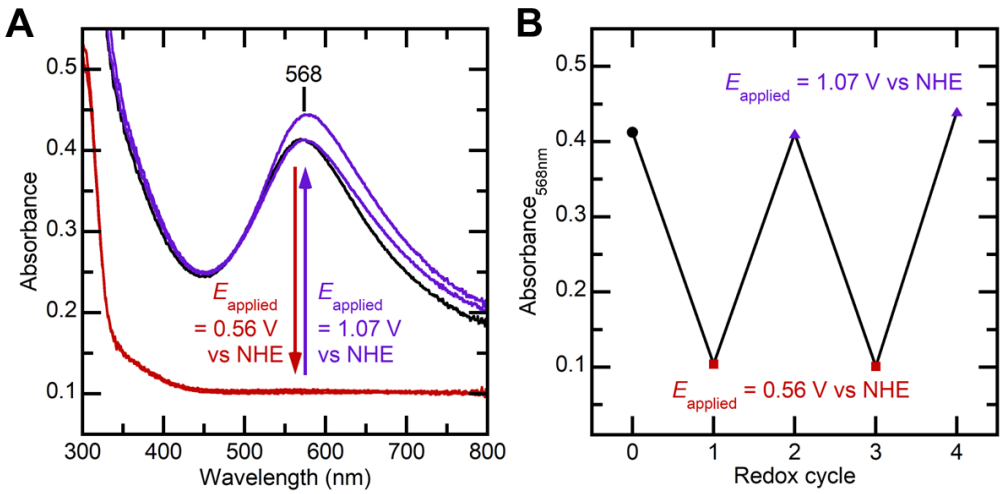

Figure S16. (**A**) Optical spectra of the NPs cycled between applied potentials of 0.56 and 1.07 V vs NHE in water (pH = 1.86, acidified by $HNO_{3(aq)}$) at room temperature. (**B**) Absorbance measurements at 568 nm of the NPs cycled between 0.56 and 1.07 V vs NHE. A boron-doped diamond electrode was used as the working electrode; Pt wire as the counter electrode; and Ag/AgCl electrode as the reference electrode.

Section S6: OAT reactivity

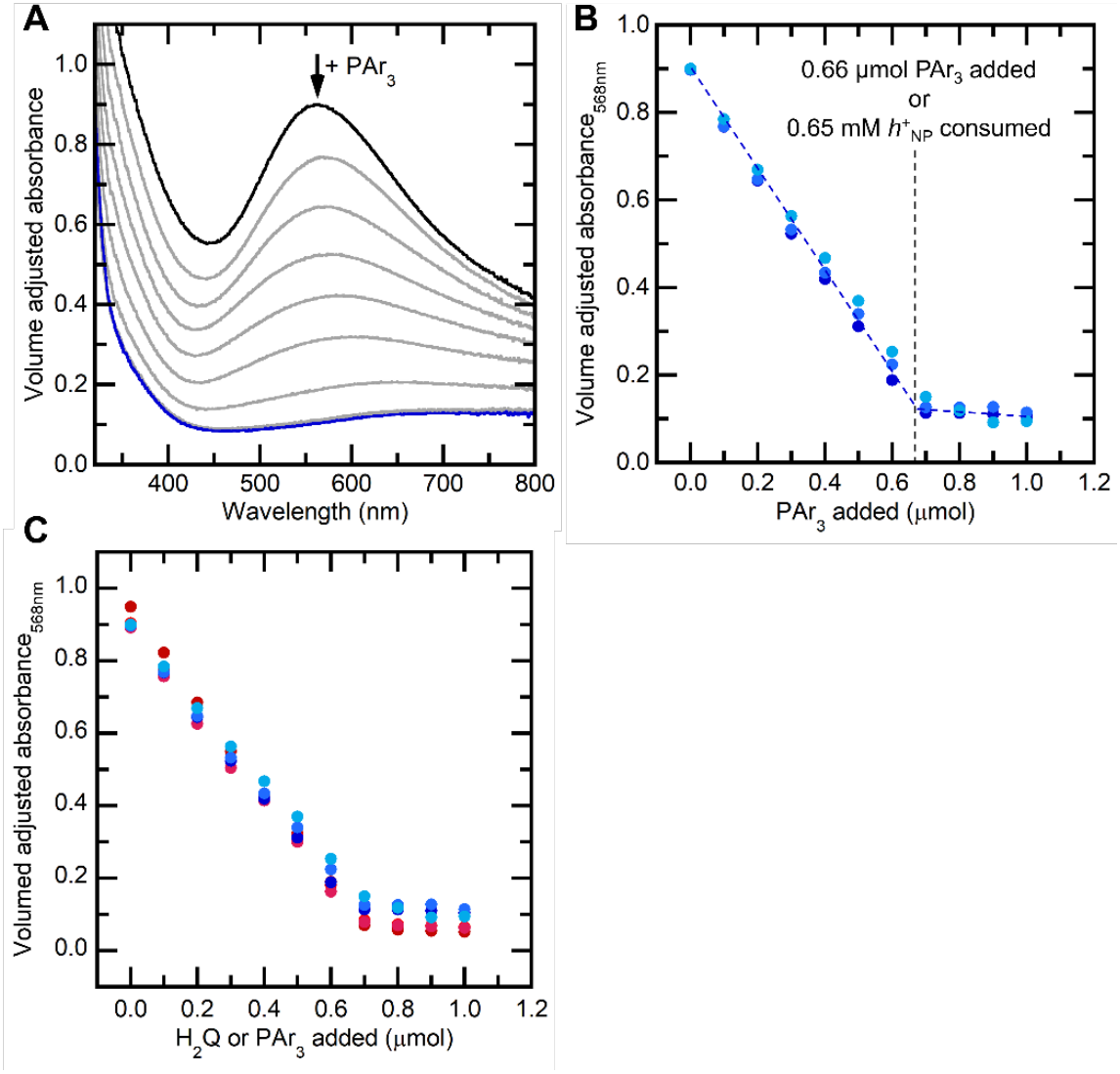

Figure S17. (**A**) UV-vis titration of IrO_x NPs in H_2O (2-fold diluted from the as-prepared NP batch) with PAr_3. Aliquots of PAr_3 (0.1 µmol) result in incremental decrease of the IrO_x optical absorbance. (**B**) Beer's law plot is used to quantify the oxidizing equivalents of IrO_x NPs. The three different shades of blue represent three separate titrations of IrO_x NPs with PAr_3. Reproduced from Lee, J. L.; Gentry, N. E.; Peper, J. L.; Hetzel, S.; Quist, C.; Menges, F. S.; Mayer, J. M. *ACS Nano* **2025**, *19*, 10289–10300. Copyright 2025 American Chemical Society.[2] (**C**) PAr_3 titration Beer's law plot triplicate comparison (blue) with H_2Q (red).

Our experimental observations show a similar pH change in the reaction of IrO_x and Par_3 as was observed with the H_2Q. Upon titrating with PAr_3, the bulk pH gradually decreased, corresponding with an additional uptake of ~0.82 µmol H^+ from the bulk solution (Figure S18). The PAr_3 overall corresponded with ~1.3 H^+ per 1e^- transfer, agreeing closely with the chemical reactivity with H_2Q in Section II.B.3 and the *electrochemical* behavior discussed in Section II.B.4.

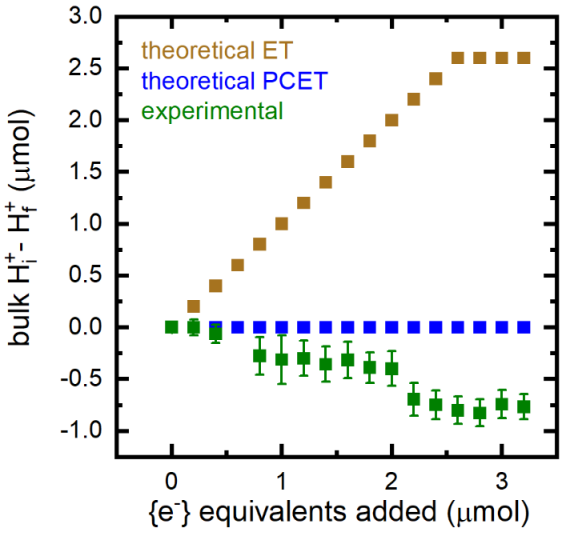

Figure S18. Change in bulk H^+ (µmol) upon the addition of H^+, e^- (µmol; ½ µmol PAr_3) calculated from pH change. Brown represents theoretical change for an ET, blue represents change for PCET, green represents experimental results. Experimental data was corrected for dilution effects.

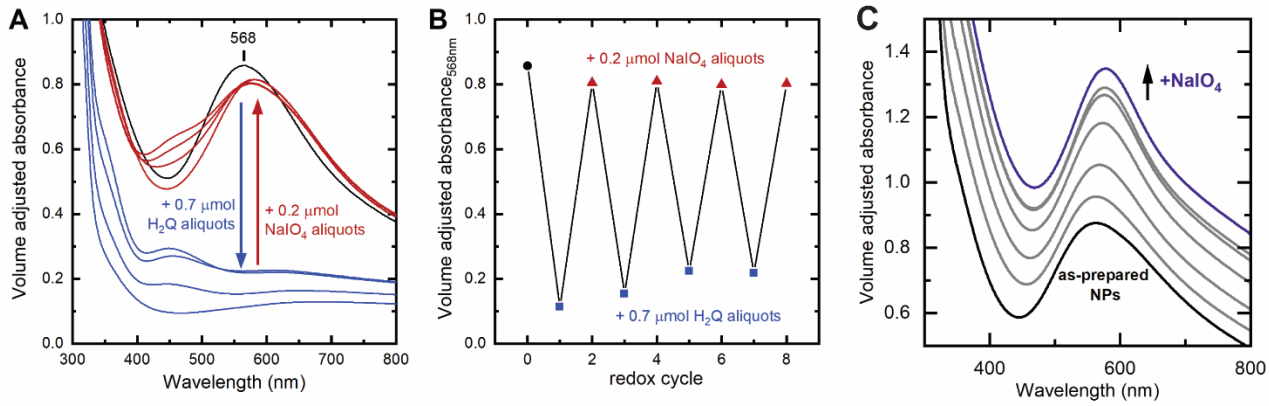

Figure S19. Redox cycling of IrO_x NPs with H_2Q as the reductant and $NaIO_4$ as the oxidant. **(**A**)** UV-vis spectra after cycles of reduction (blue arrow and spectra) and oxidation (red arrow and spectra). **(**B**)** Corrected absorbances after successive cycles of reduction (blue) then oxidation (red). **(**C**)** UV-vis spectra of as-prepared IrO_x NPs further oxidized with aliquots of $NaIO_4$ (0.1 µmol).

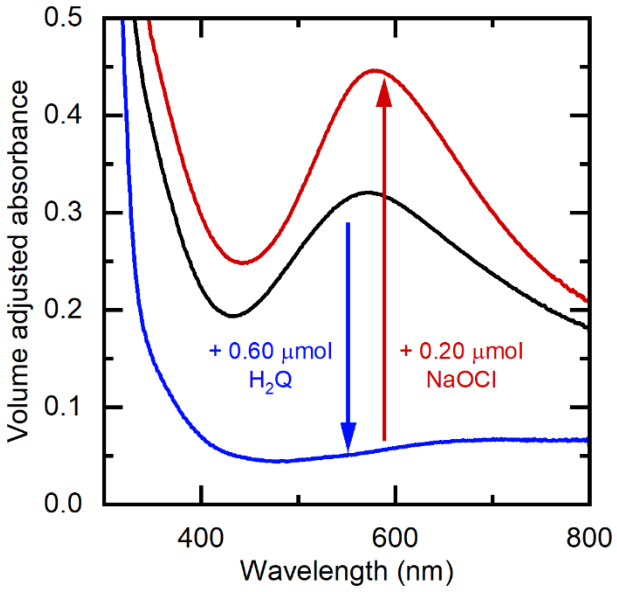

Figure S20. UV-vis spectra of IrO_x NPs upon reduction with H_2Q (blue arrow and spectra) and oxidation with NaOCl (red arrow and spectra), demonstrating that the NPs can be further oxidized above $Ir^{3.8+}$ using NaOCl.

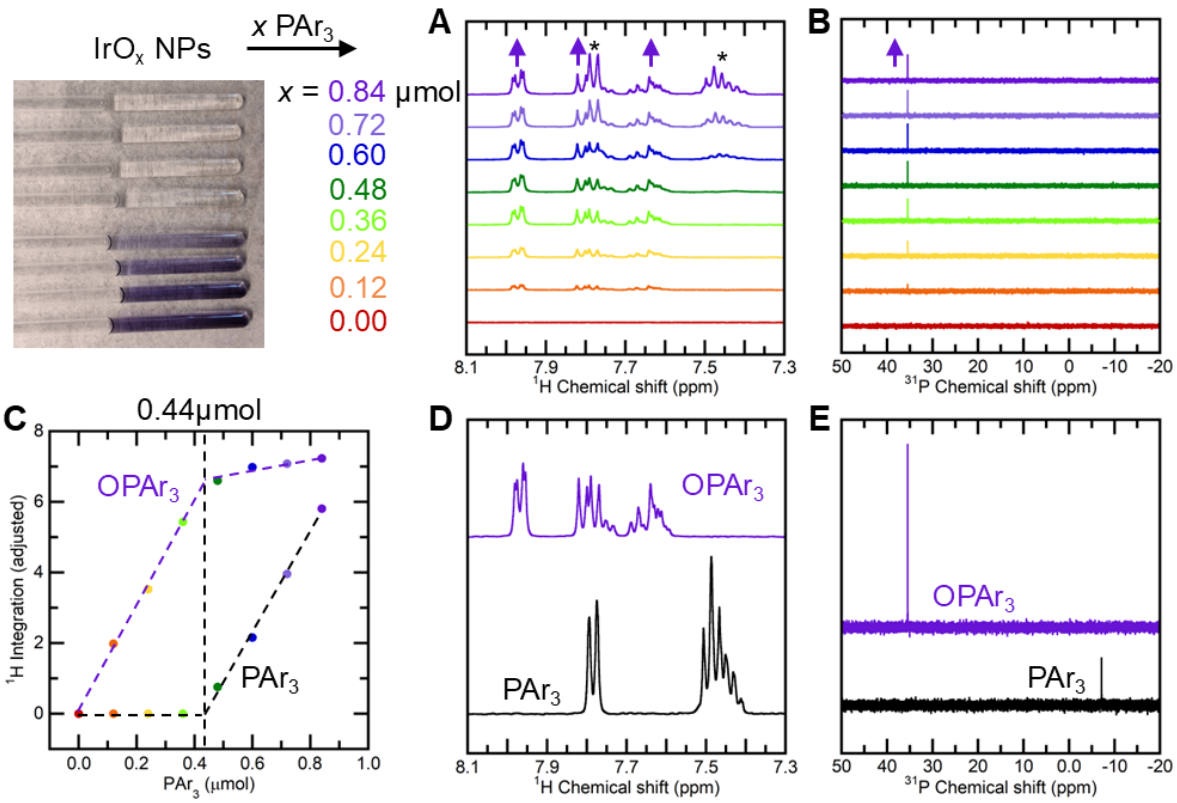

Figure S21. NMR titrations of IrO_x NPs with aliquots (0.12 µmol) of PAr_3; the solvent was 85:15 H_2O:D_2O; $(CH_3)_2SO_2$ was used as an internal chemical shift (δ 3.14 ppm) and quantification reference. Addition of PAr_3 results in the growth of the $OPAr_3$ features (indicated by the purple arrows) in the ^1H (**A**) and ^{31}P (**B**) NMR spectra. The asterisks (*) indicate excess PAr_3. The integrations of the δ 7.95 ppm feature for $OPAr_3$ and δ 7.45 ppm feature for PAr_3 are adjusted by the appropriate integrated Hs (4H and 9H, respectively), and then plotted in a Beer's law plot to quantify the oxidizing equivalents of IrO_x (**C**). The ^1H (**D**) and ^{31}P (**E**) NMR spectra of the PAr_3 (black, 1.4 mM) and $OPAr_3$ (purple, 1.4 mM) standards. The solvent was 93:7 H_2O:D_2O. $(CH_3)_2SO_2$ was used as an internal chemical shift (δ 3.14 ppm) reference. Reproduced from Lee, J. L.; Gentry, N. E.; Peper, J. L.; Hetzel, S.; Quist, C.; Menges, F. S.; Mayer, J. M. *ACS Nano* **2025**, *19*, 10289–10300.[2] Copyright 2025 American Chemical Society.

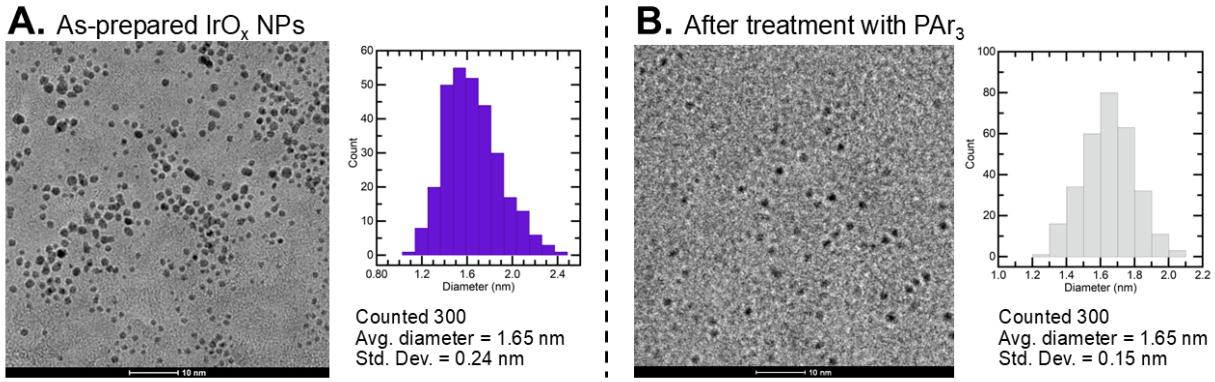

Figure S22. TEM images of the IrO_x NPs before (**A**) and after (**B**) treatment with PAr_3 (750 µL of the as-prepared IrO_x solution + 0.75 µmol PAr_3, 1.1 equiv. PAr_3 using the 2 oxidizing equivalents : 1 PAr_3 ratio) after 2 days. No significant change to NP size was observed. The scale bars are 10 nm. Reproduced from Lee, J. L.; Gentry, N. E.; Peper, J. L.; Hetzel, S.; Quist, C.; Menges, F. S.; Mayer, J. M. *ACS Nano* **2025**, *19*, 10289–10300.[2] Copyright 2025 American Chemical Society.

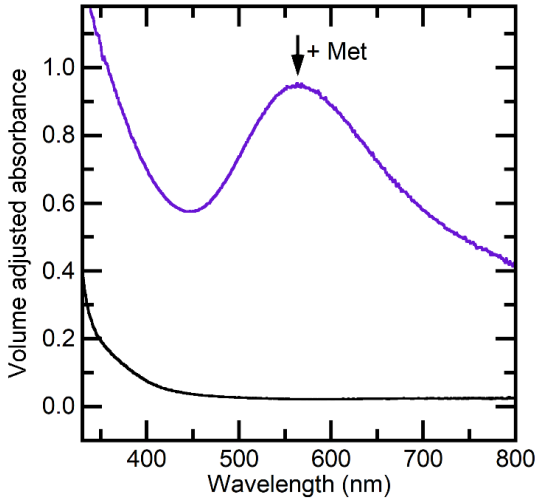

Figure S23. UV-vis measurements of before (purple) and after (black) the reaction of IrO_x NPs with 1.0 equiv. Met (0.8 µmol) in H_2O (pH 1.9) over 14 days. Reproduced from Lee, J. L.; Gentry, N. E.; Peper, J. L.; Hetzel, S.; Quist, C.; Menges, F. S.; Mayer, J. M. *ACS Nano* **2025**, *19*, 10289–10300.[2] Copyright 2025 American Chemical Society.

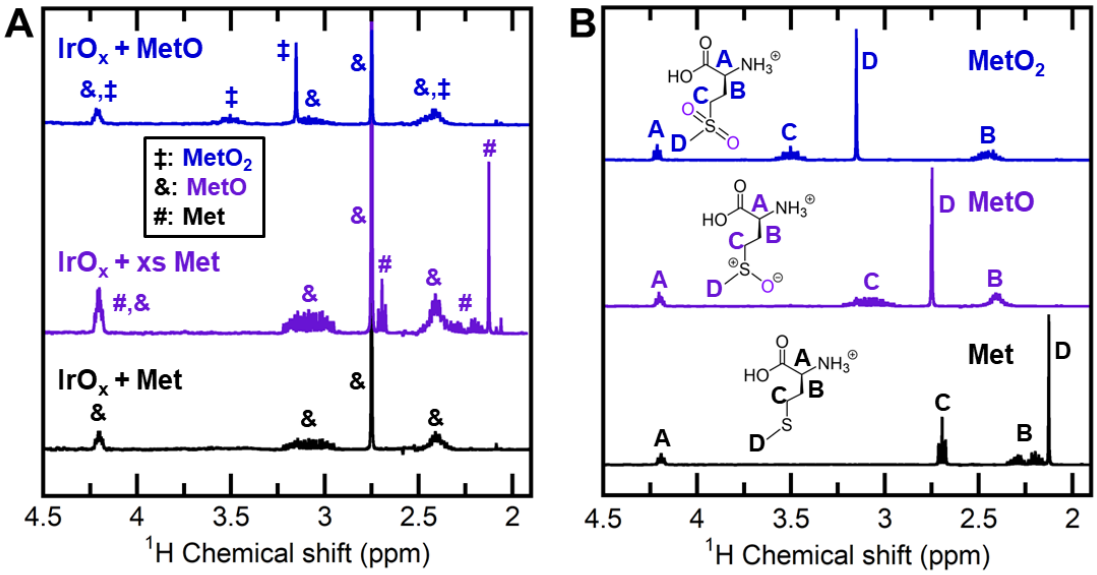

Figure S24. (**A**) NMR measurements of IrO_x NPs reactions with sub-stoichiometric Met (0.7 equiv., 0.15 μmol, black), excess Met (1.4 equiv., 0.30 μmol, purple), and sub-stoichiometric MetO (0.7 equiv., 0.15 μmol, blue) after 9 days; $(CH_3)_3COH$ was used as an internal chemical shift (δ 1.24 ppm) and quantification reference. Addition of Met results in growth of the MetO features (indicated by &) in the ^1H NMR spectrum (black). # indicates excess Met (purple). Addition of MetO (blue) results in the growth of the $MetO_2$ features (‡). (**B**) ^1H NMR spectra of the Met (black), MetO (purple), and $MetO_2$ (blue) standards at concentrations of 0.45 mM. The solvent was 75:25 H_2O:D_2O with a pH of ~1.7 (acidified by HNO_3 (aq)). Reproduced from Lee, J. L.; Gentry, N. E.; Peper, J. L.; Hetzel, S.; Quist, C.; Menges, F. S.; Mayer, J. M. *ACS Nano* **2025**, *19*, 10289–10300.[2] Copyright 2025 American Chemical Society.

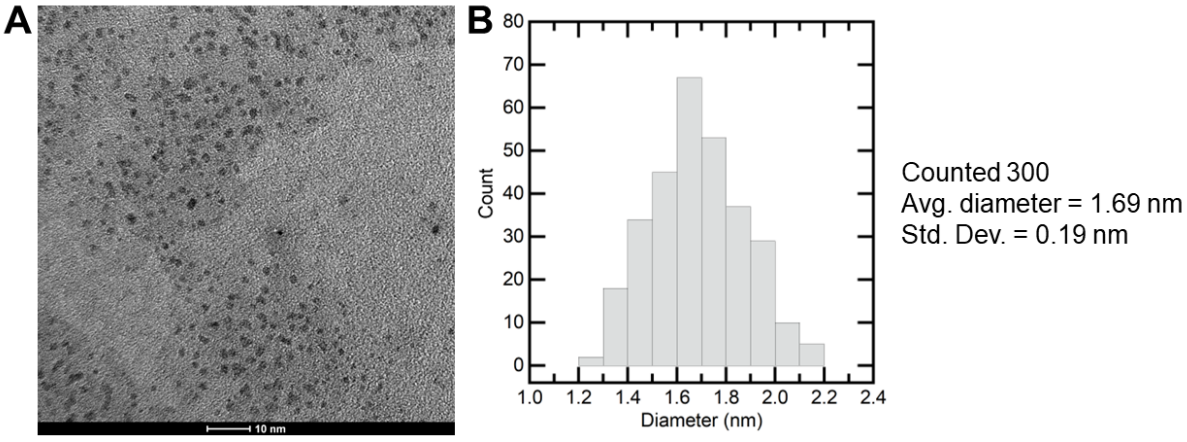

Figure S25. (**A**) TEM image of the IrO_x NPs (500 μL of the as-prepared solution) after treatment with Met (0.75 μmol, 2.3 equiv. using the 2 oxidizing equivalents : 1 Met ratio) for 9 days. The scale bar is 10 nm. (**B**) The size distribution of the NPs. No significant change to NP size was observed. Reproduced from Lee, J. L.; Gentry, N. E.; Peper, J. L.; Hetzel, S.; Quist, C.; Menges, F. S.; Mayer, J. M. *ACS Nano* **2025**, *19*, 10289–10300.[2] Copyright 2025 American Chemical Society.

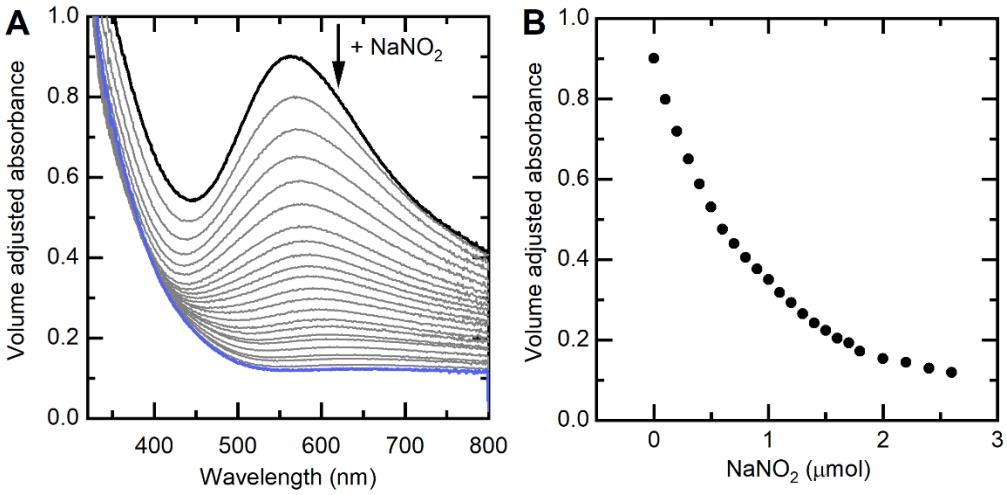

Figure S26. (**A**) UV-vis titration of IrO_x NPs in H_2O (2-fold diluted from the as-prepared NP batch) with $NaNO_2$. Aliquots of $NaNO_2$ (0.1 μmol) result in incremental decrease of the IrO_x optical absorbance. (**B**) Absorbance (volume adjusted) vs. nitrite added shows no clear titration endpoint.

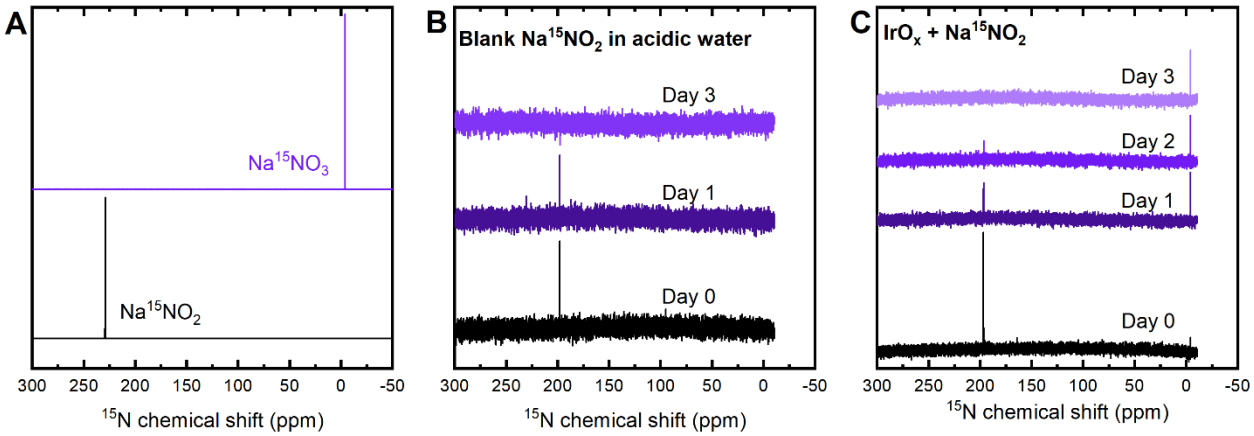

Figure S27. (**A**) ^{15}N NMR of 1 M $Na^{15}NO_2$ (black, δ 229 ppm) and $Na^{15}NO_3$ (purple, δ –4.04 ppm) standards in D_2O. (**B**) ^{15}N NMR of 20 mM $Na^{15}NO_2$ in D_2O with a pH ~ 1.8 (acidified by HNO_3) measured over three days. The upfield shift of the $^{5}NO_2^-$ to δ 197 ppm is likely due to the formation of nitrous acid at this pH, followed by nitrosation,[7] as observed by the gradual disappearance of the NMR feature over 3 days. (**C**) ^{15}N NMR of IrO_x NPs with 20 mM excess $Na^{15}NO_2$ measured over 3 days. The growth of the δ –4.24 ppm is suggestive of the formation of the $^{15}NO_3^-$ product.

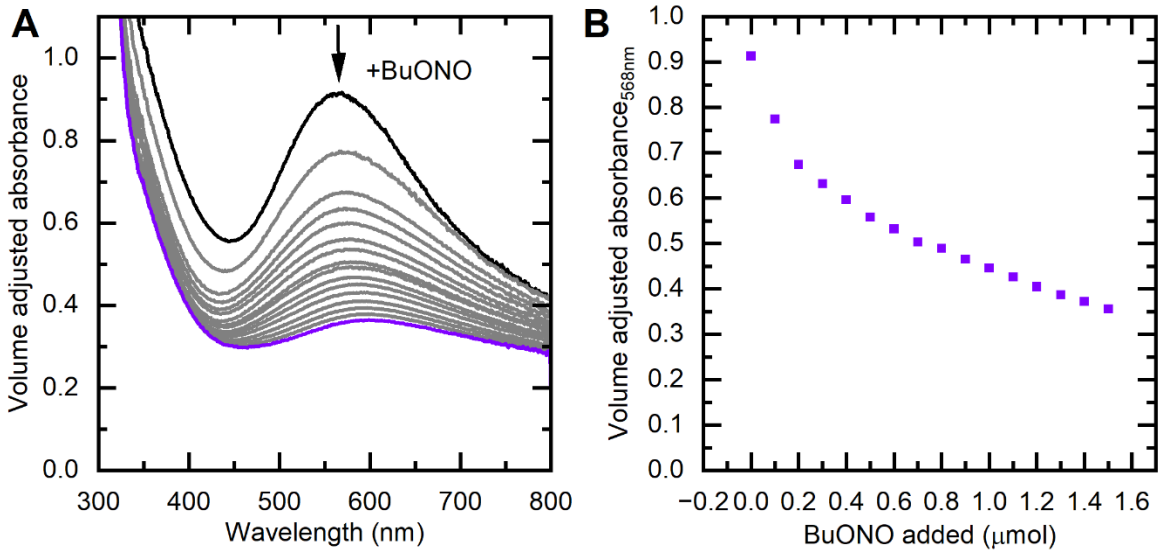

Figure S28. (A)UV-vis titration of IrO_x NPs in H_2O (2-fold diluted from the as-prepared NP batch) with *n*-butyl nitrate (BuONO). Aliquots of BuONO (0.1 μmol) result in little change in absorbance. Initial scan (black) and final scan (purple) were collected four months apart. (**B**) Absorbance (volume adjusted) vs. BuONO added shows no titration endpoint.

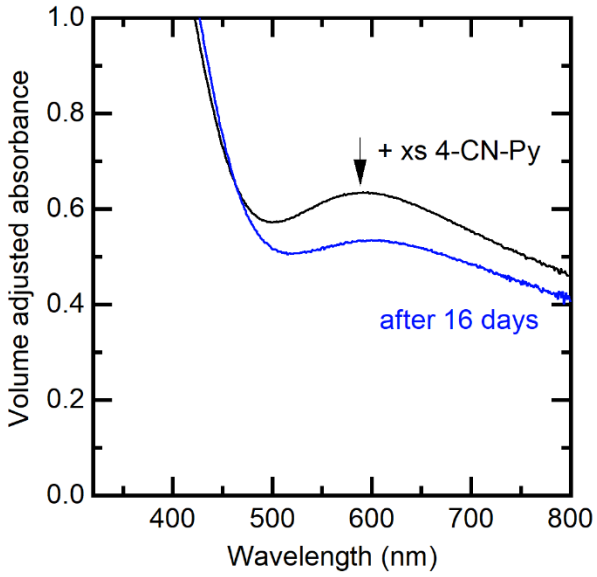

Figure S29. UV-vis titration of IrO_x NPs in H_2O (2-fold diluted from the as-prepared NP batch) with an excess of 20 mM 4-CN-pyridine (20 μmol) showing little change in absorbance after 16 days.

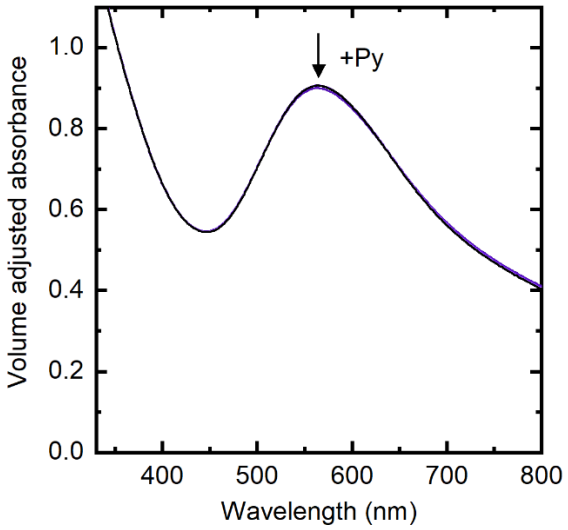

Figure S30. UV-vis titration of IrO_x NPs in H_2O (2-fold diluted from the as-prepared NP batch) with pyridine showing little change in absorbance.

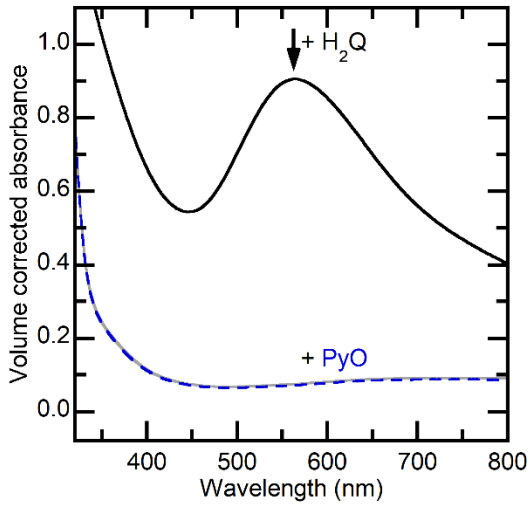

Figure S31. UV-vis measurements of before (black) and after (gray) the reaction of IrO_x NPs with 1.0 equiv. H_2Q (0.7 μmol) in H_2O (pH 1.9), then with 1.3 equiv. pyO (0.9 μmol; blue dashed line). No reaction was observed between the reduced IrO_x NPs and pyO over 2 hours.

Section S7: Bond dissociation enthalpies (BDEs) and bond dissociation free energies (BDFEs) for Y–O substrates

Holm and Donahue compiled a large and valuable list of heats and free energies for the oxygenation of Y + ½ $O_{2(g)}$ to YO (eq. S11, $\Delta H_{Y/YO}$ and $\Delta G_{Y/YO}$), Table S1 below. For a Y/YO couple, $\Delta H_{Y/YO}$ and $\Delta G_{Y/YO}$ are the differences in the standard molar *enthalpies* or *free energies* of formation of YO and Y, respectively (eq. S11), because the $\Delta_f H°$ and $\Delta_f G°$ of $O_{2(g)}$ are by convention zero.

$$Y_{(g/l/s/aq)} + ½\ O_{2(g)} \rightleftarrows Y\text{–}O_{(g/l/s/aq)} \qquad \Delta H_{Y/YO} \text{ or } \Delta G_{Y/YO} \qquad \text{eq. S11}$$

Table S1. Table of $\Delta G_{Y/YO}$ and $\Delta H_{Y/YO}$ values for various Y/YO couples.[a,b]

Y	YO	$\Delta G_{Y/YO}$	$\Delta H_{Y/YO}$	$\Delta G_{Y/YO} - \Delta H_{Y/YO}$
$H_2O_{(l)}$	H_2O_2	+27.9	+23.4	+4.5
$BrO_3^-{}_{(aq)}$	BrO_4^-	+23.8	+19.1	+4.7
$KBrO_{3(s)}$	$KBrO_4$	+23.1	+17.3	+5.8
$Cl^-{}_{(aq)}$	ClO^-	+22.6	+14.4	+8.2
$K_2S_2O_{7(s)}$	$K_2S_2O_8$	+22.5	+16.8	+5.7
$OH^-{}_{(aq)}$	HO_2^-	+21.5	+16.7	+4.8
$Br^-{}_{(aq)}$	BrO^-	+16.9	+6.56	+10.34
$IO_3^-{}_{(aq)}$	IO_4^-	+16.6	+16.7	–0.1
$KIO_{3(s)}$	KIO_4	+13.6	+8.16	+5.44
$ClO^-{}_{(aq)}$	ClO_2^-	+12.9	+9.70	+3.2
$I^-{}_{(aq)}$	IO^-	+3.12	–12.5	+15.62
$NaClO_{3(s)}$	$NaClO_4$	+1.8	–4.9	+6.7
$ClO_3^-{}_{(aq)}$	ClO_4^-	–0.14	–6.06	+5.92
$ClO_2^-{}_{(aq)}$	ClO_3^-	–6.00	–8.95	+2.95
$HSeO_3^-{}_{(aq)}$	$HSeO_4^-$	–9.76	–16.0	+6.24
$AgNO_{2(s)}$	$AgNO_3$	–12.6	–19.0	+6.4
$SeO_3^{2-}{}_{(aq)}$	SeO_4^{2-}	–17.1	–21.5	+4.4
$Na_2O_{(s)}$	Na_2O_2	–17.3	–23.1	+5.8
$S_2O_3^{2-}{}_{(aq)}$	$S_2O_4^{2-}$	–18.7	–24.3	+5.6
$NO_2^-{}_{(aq)}$	NO_3^-	–18.9	–24.0	+5.1
$NaNO_{2(s)}$	$NaNO_3$	–19.7	–26.1	+6.4
$V_2O_{4(s)}$	V_2O_5	–24.2	–29.5	+5.3
$MnO_{(s)}$	MnO_2	–24.4	–32.2	+7.8
$Me_2S_{(l)}$	Me_2SO	–25.1	–33.0	+7.9
$ReO_{2(s)}$	ReO_3	–27	–34	+7
$MoO_{2(s)}$	MoO_3	–32.3	–37.3	+5.0
$MoBr_{3(s)}$	$MoOBr_3$	–39	–49	+10
$H_2AsO_3^-{}_{(aq)}$	$H_2AsO_4^-$	–39.7	–46.6	+6.9
$V_2O_{3(s)}$	V_2O_4	–42.8	–49.8	+7.0
$HSO_3^-{}_{(aq)}$	HSO_4^-	–54.5	–62.4	+7.9
$WO_{2(s)}$	WO_3	–55.0	–60.5	+5.5
$HCO_2^-{}_{(aq)}$	HCO_3^-	–56.3	–63.7	+7.4
$Na_2SO_{3(s)}$	Na_2SO_4	–61.6	–68.4	+6.8
$SO_3^{2-}{}_{(aq)}$	SO_4^{2-}	–61.7	–65.4	+3.7
$GeO_{(s)}$	GeO_2	–62.1	–69.1	+7.0
$MeCHO_{(l)}$	$MeCO_2H$	–62.4	–69.8	+7.4
$SnO_{(s)}$	SnO_2	–62.8	–70.5	+7.7
$CN^-{}_{(aq)}$	OCN^-	–64.5	–70.9	+6.4
$GaCl_3{\bullet}PCl_{3(s)}$	$GaCl_3{\bullet}POCl_3$	–65	–71	+6
$UCl_{3(s)}$	$UOCl_3$	–65.0	–70.9	+5.9
$NaH_{(s)}$	NaOH	–82.7	–88.3	+5.6

[a] All data from reference 8. [b] All energies in kcal mol^{-1}.

For gas-phase and solution reactions, we prefer to use BDEs and BDFEs rather than heats of oxygenation. The differences between the $\Delta H_{Y/YO}$ and the BDE, or the $\Delta G_{Y/YO}$ and the BDFE, are the enthalpy or free energy of formation of O in the gas or solution phase (eq S12, 13). In some cases, Holm and Donahue tabulated $\Delta H_{Y/YO}$ and/or $\Delta G_{Y/YO}$ for the pure liquid or solid Y and YO. These cannot simply be converted to a BDE or BDFE because there is no simple definition of O in the pure liquid or solid phase.

$Y–O_{(g/aq)} \rightleftarrows Y_{(g/aq)} + O_{(g/aq)}$	$BDE[Y–O] = –\Delta H_{Y/YO} + \Delta_f H°(O_{(g/aq)})$ $BDFE[Y–O] = –\Delta G_{Y/YO} + \Delta_f G°(O_{(g/aq)})$	eq. S12
$½\ O_{2(g)} \rightleftarrows O_{(g)}$	$\Delta_f H°(O_{(g)}) = 59.6$ kcal mol^{-1} [8] $\Delta_f G°(O_{(g)}) = 55.4$ kcal mol^{-1} [8]	eq. S13

We note that all energy values in this section are given in kcal mol^{-1}, so that unit will be omitted in most cases below.

The free energy of solvation O atom from the gas phase to an aqueous solution is estimated using equations S14-18. Therefore, the $\Delta_f G°(O_{(aq)}) = \Delta_f G°(O_{(g)}) + \Delta G°_{O,solvation} \cong 61.7$ kcal mol^{-1}.

$O_{(g)} + 2\ H•_{(g)} \rightleftarrows H_2O_{(g)}$	$–\Delta G°_{H2O(g),atomization} = –205.2$ [9]	eq. S14
$2\ H•_{(aq)} \rightleftarrows 2\ H•_{(g)}$	$–2\Delta G°_{H•,solvation} = 2*(48.6–52.8) = –8.4$ [9]	eq. S15
$H_2O_{(l)} \rightleftarrows O_{(aq)} + 2\ H•_{(aq)}$	$\Delta G°_{H2O(l),atomization} = 217.8$ [9]	eq. S16
$H_2O_{(g)} \rightleftarrows H_2O_{(l)}$	$\Delta G°_{H2O,solvation} = –54.6–(–56.7) = 2.1$ [10]	eq. S17
$O_{(g)} \rightleftarrows O_{(aq)}$	$\Delta G°_{O,solvation} \cong 6.3$ kcal mol^{-1}	eq. S18

This analysis provides the BDFE(Y-O) in gas or aqueous media from the $–\Delta G_{Y/YO}$ in that medium (eqs. S19 and S20).

$Y–O_{(g)} \rightleftarrows Y_{(g)} + O_{(g)}$	$BDFE[Y–O_{(g)}] = –\Delta G_{Y/YO(g)} + 55.4$	eq. S19
$Y–O_{(aq)} \rightleftarrows Y_{(aq)} + O_{(aq)}$	$BDFE[Y–O_{(aq)}] = –\Delta G_{Y/YO(aq)} + 61.7$	eq. S20

For many OAT couples, the $\Delta H_{Y/YO}$ has been reported but not the $\Delta G_{Y/YO}$. For any reaction (at constant T and P), $\Delta G = \Delta H – T\Delta S$. With the rough assumption that the $\Delta S°$ values for Y and YO are the same, the difference between the $\Delta G°$ and the $\Delta H°$ is $– T\Delta S°(O)$. For $O_{(g)}$, $T\Delta S° = 298.15$ K • [38.4940 ± 0.0007 (cal/mol•K)][10,11] = 11.5 kcal mol^{-1}. Then:

$Y–O_{(g)} \rightleftarrows Y_{(g)} + O_{(g)}$	$BDFE[Y–O_{(g)}] \cong BDE[Y–O_{(g)}] – 11.5$	eq. S21

To derive BDFEs from BDEs in solution requires the entropy of solvation of O atom, which can be roughly estimated with the value for an Ar atom: $– T\Delta S°(Ar) = – 298.15$ K • (–0.022881) = 6.8 kcal mol^{-1}.[10] This gives:

$$Y{-}O_{(aq)} \rightleftarrows Y_{(aq)} + O_{(aq)} \qquad BDFE[Y{-}O_{(aq)}] \cong -\Delta G_{Y/YO(aq)} + 61.7 + 6.8 \qquad \text{eq. S22}$$

Another way to estimate the typical BDE/BDFE difference for condensed-phase YO species is to compare known values. Table S1 lists 41 examples,[8] and the calculated an average $[\Delta G_{Y/YO}–\Delta H_{Y/YO}]$ difference of 6.5 ± 2.1 kcal mol^{-1} (eq. S23), in good agreement with the above approximation that the entropy term contributes little to the calculated BDFE.

$$Y_{(g/l/s/aq)} + \tfrac{1}{2}\, O_{2(g)} \rightleftarrows Y{-}O_{(g/l/s/aq)} \qquad \Delta G_{Y/YO} = \Delta H_{Y/YO} + (6.5 \pm 2.1) \qquad \text{eq. S23}$$

The BDFE of a Y–O reagent, with a known $\Delta H_{Y/YO}$ value and an unknown $\Delta G_{Y/YO}$, can then be estimated (eq. S24).

$$Y{-}O_{(aq)} \rightleftarrows Y_{(aq)} + O_{(aq)} \qquad BDFE[Y{-}O_{(aq)}] \cong -\Delta H_{Y/YO(aq)} + 55 \qquad \text{eq. S24}$$

The solution BDFEs of the Y–O substrates used in this study were calculated using eq. S23 or S24, and are listed in Table S2. For substrates with both known $\Delta G_{Y/YO}$ and $\Delta H_{Y/YO}$ values, $\Delta G_{Y/YO}$ and eq. S23 were used to calculate the BDFE[Y–O].

Table S2. Tabulation of the Y–O substrates used in this study and their thermochemical values.[a]

Y	YO	$\Delta G_{Y/YO}$	$\Delta H_{Y/YO}$	BDFE[Y–O] calc'd from $\Delta G_{Y/YO\ (g)}$	BDFE[Y–O] calc'd from $\Delta H_{Y/YO}$	IrO_x + Y reaction direction	Refer-ence
HSO_4^-	HSO_5^-	n.d.	n.d.	n.d.	n.d.	←	
IO_3^-	IO_4^-	+16.6	+16.7	45.1	38.5 ± 2.1	←	8
Cl^-	ClO^-	+22.6	+14.4	39.1	40.4 ± 2.1	←	8
Py	pyO	n.d.	–3.8	n.d.	59.0 ± 2.1	nr	12
4-CN-py	4-CN-pyO	n.d.	–3.9	n.d.	59.1 ± 2.1	nr	12
BuONO [b]	$BuONO_2$	n.d.	–14.7	n.d.	69.9 ± 2.1	nr	8
NO_2^-	NO_3^-	–18.9	–24.0	80.6	79.2 ± 2.1	→	8
Met [c]	MetO	–25.1	–33.0	86.8	88.2 ± 2.1	→	8
MetO [d]	$MetO_2$	–45.7	–52.7	107.4	107.9 ± 2.1	→	8
PAr_3 [e]	$OPAr_3$	n.d.	–69.9	n.d.	125.1 ± 2.1	→	8

[a] BDFE values in kcal mol^{-1}. All materials in aqueous solution. n.d. = Not determined. [b] Assumed to be the same as $EtONO_2$. [c] Assumed to be the same as $Me_2S(O)$. [d] Assumed to be the same as Me_2SO_2. [e] Assumed to be the same as $OPPh_3$. For reaction IrO_x + Y, the symbol → indicates that the reaction proceeds left to right forming the reduced-IrO_x and YO product. "nr" indicates that no reaction was observed. The symbol ← indicates that the reaction proceeds right to left: reduced-IrO_x + YO forms Y + oxidized-IrO_x.

Section S8: References

(1) Zhao, Y.; Hernandez-Pagan, E. A.; Vargas-Barbosa, N. M.; Dysart, J. L.; Mallouk, T. E. A High Yield Synthesis of Ligand-Free Iridium Oxide Nanoparticles with High Electrocatalytic Activity. *Journal of Physical Chemistry Letters* **2011**, *2* (5), 402–406. https://doi.org/10.1021/jz200051c.

(2) Lee, J. L.; Gentry, N. E.; Peper, J. L.; Hetzel, S.; Quist, C.; Menges, F. S.; Mayer, J. M. Oxygen Atom Transfer Reactions of Colloidal Metal Oxide Nanoparticles. *ACS Nano* **2025**, *19* (10), 10289–10300. https://doi.org/10.1021/acsnano.4c17955.

(3) Rogers, D. B.; Shannon, R. D.; Sleight, A. W.; Gillson, J. L. Crystal Chemistry of Metal Dioxides with Rutile-Related Structures. *Inorganic Chemistry* **1969**, *8* (4), 841–849. https://doi.org/10.1021/ic50074a029.

(4) Creutz, C. Complexities of Ascorbate as a Reducing Agent. *Inorg. Chem.* **1981**, *20* (12), 4449–4452. https://doi.org/10.1021/ic50226a088.

(5) Kerber, R. C. "As Simple as Possible, but Not Simpler"—The Case of Dehydroascorbic Acid. *J. Chem. Educ.* **2008**, *85* (9), 1237–1242. https://doi.org/10.1021/ed085p1237.

(6) Njus, D.; Kelley, P. M.; Tu, Y.-J.; Schlegel, H. B. Ascorbic Acid: The Chemistry Underlying Its Antioxidant Properties. *Free Radical Biology and Medicine* **2020**, *159*, 37–43. https://doi.org/10.1016/j.freeradbiomed.2020.07.013.

(7) Yost, D. M.; Russell, Jr., H. Nitrogen and Its Oxides and Sulfides. In *Systematic inorganic chemistry of the fifth-and-sixth-group nonmetallic elements*; New York, Prentice-Hall, Inc., 1946; pp 1–40.

(8) Holm, R. H.; Donahue, J. P. A Thermodynamic Scale for Oxygen Atom Transfer Reactions. *Polyhedron* **1993**, *12* (6), 571–589. https://doi.org/10.1016/S0277-5387(00)84972-4.

(9) Agarwal, R. G.; Coste, S. C.; Groff, B. D.; Heuer, A. M.; Noh, H.; Parada, G. A.; Wise, C. F.; Nichols, E. M.; Warren, J. J.; Mayer, J. M. Free Energies of Proton-Coupled Electron Transfer Reagents and Their Applications. *Chemical Reviews* **2022**, *122* (1), 1–49. https://doi.org/10.1021/acs.chemrev.1c00521.

(10) Wagman, D. D.; Evans, W. H.; Parker, V. B.; Schumm, R. H.; Halow, I.; Bailey, S. M.; Churney, K. L.; Nuttall, R. L. The NBS Tables of Chemical Thermodynamic Properties: Selected Values for Inorganic and C_1 and C_2 Organic Substances in SI Units. *Journal of Physical and Chemical Reference Data* **1982**, *11* (2).

(11) Linstrom, Eds. P. J.; Mallard, W. G. NIST Chemistry WebBook, NIST Standard Reference Database 69, 1997. https://doi.org/10.18434/T4D303.

(12) Ribeiro Da Silva, M. D. M. C.; Agostinha, M.; Matos, R.; Vaz, M. C.; Santos, L. M. N. B. F.; Pilcher, G.; Acree Jr., W. E.; Powell, J. R. Enthalpies of Combustion of the Pyridine N-Oxide Derivatives: 4-Methyl-, 3-Cyano-, 4-Cyano-, 3-Hydroxy-, 2-Carboxy-, 4-Carboxy-, and 3-Methyl-4-Nitro, and of the Pyridine Derivatives: 2-Carboxy-, and 4-Carboxy-. The Dissociation Enthalpies of the N-O Bonds. *The Journal of Chemical Thermodynamics* **1998**, *30* (7), 869–878. https://doi.org/10.1006/jcht.1998.0353.